Plasmonic enhancement of one-photon- and two-photon-excited single-molecule fluorescence by single gold nanorods

Zhang, W.

4

Enhancement of hot-band absorption anti-Stokes luminescence of single molecules by individual gold nanorods

Frequency upconversion luminescence is an optical process that converts long-wavelength excitation to short-wavelength emission. Upconversion materials are especially suited for bio-imaging applications because anti-Stokes shift luminescence leads to reduced background from auto-fluorescence of biological tissues. Here we demonstrate anti-Stokes luminescence from a commercial squaraine dye, Seta 670. The luminescence is induced by optical absorption from a vibrational hot-band. We use individual chemically-synthesized gold nanorods to enhance the anti-Stokes emission intensity of single Seta 670 molecules and obtain an enhancement factor of 350.

4.1. Introduction

Fluorescence-based light microscopy continues to develop as an indispensable tool in material science and biology because of, among others, its high contrast since photons are emitted at a different wavelength than the excitation photons. Specially, fluorescence microscopy has the sensitivity of detecting exceedingly low concentrations of molecules, down to the single-molecule level. Demonstration of optical detection of single-molecule fluorescence marked a major breakthrough in the field of optics [1]. It greatly extended the scope of fluorescent microscopy, providing unprecedented insights into complex systems where static and dynamic heterogeneity is present [2–4].

Over the decades, imaging probes of various kinds have been developed, including synthetic organic dyes, fluorescent biomolecules (notably green fluorescent proteins), and semiconductor nanocrystals. Recently, frequency upconversion materials have attracted much attention because of the anti-Stokes shift of the emission wavelength with respect to the excitation wavelength. This feature makes them especially interesting for bio-imaging applications because of the reduced background from auto-fluorescence of biological tissues. Moreover, upconversion emission usually involves near-infrared (NIR) excitation, which has a larger penetration depth into tissues. Three different materials and mechanisms can generate anti-Stokes emission [5] (i) multi-photon absorption, which usually requires femtosecond pulsed lasers for extremely high excitation energy. (ii) lanthanide- and triplet-triplet annihilation-based upconversion nanoparticles; (iii) hot-band absorption induced luminescence, where a molecule is excited to the lowest excited state from a higher vibrational energy level (termed "hot band") and emit photons whose wavelength is shorter than that of the excitation photons. The mechanism is illustrated in Fig. 4.1(a) with a Jablonski diagram. In hot-band absorption induced luminescence, the additional energy is provided by thermal energy, therefore hot-band absorption is usually accompanied by a concomitant decrease in the temperature of the system. Such a feature gives rise to applications in laser cooling [6, 7]. Hot-band absorption is a linear process, which does not require expensive ultrafast lasers. Hot-band absorption anti-Stokes luminescent materials are typical dye molecules. Their nanometer size features a major advantage as fluorescent probes over bulky optical probes such as quantum dots, metal nanoparticles and upconversion nanoparticles in that they have minimum effects on the motion, localization and interactions of tagged objects, which is highly desired for fluorescence correlation spectroscopy, single-molecule imaging, *etc*. However, the application of this anti-Stokes luminescence in microscopy is hampered by its low efficiency, *i.e.*, low luminescence brightness. Only a limited number of dyes have demonstrated hot-band absorption anti-Stokes emission [5, 8], mainly because there is no rational rule for designing such molecules with better brightness.

It has been long known that metallic nanostructures, such as nanospheres [9], bow-ties [10] or nanorods [11, 12], are able to enhance the fluorescence emission of a single adjacent molecule. The gain in the detected fluorescence arises from the combined excitation and emission rate enhancement. The former comes form the highly concentrated electric fields produced around these nanostructures due to the resonant excitation of surface plasmons [13], while the later arises from the modification of the radiative decay rate [9], similar to the effect of a metallic surface [14]. In the present work, we demonstrate the possibility of enhancing hot-band absorption induced luminescence by chemically synthesized gold

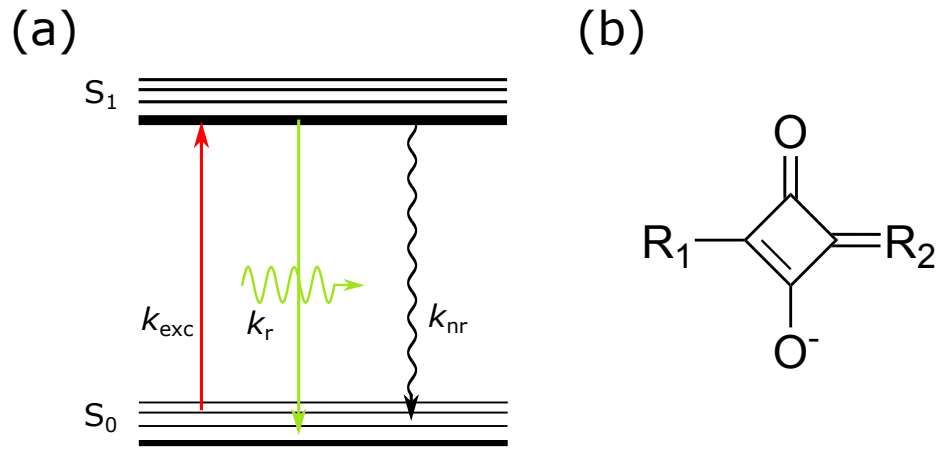

Figure 4.1: (a) Jablonski diagram illustrating the mechanism of hot-band absorption induced luminescence. k_{exc}: excitation rate; k_{r}: radiative rate; k_{nr}: nonradiative rate; (b) General chemical structure of squaraine dyes.

nanorods. The molecule in our study is a commercial squaraine dye, Seta 670. Squaraines are a class of fluorophores with a characteristic squarylium core flanked by nucleophilic motifs (Fig. 4.1(b)). They are extensively used for fluorescent labeling because of their strong red/NIR absorption and emission and excellent photostability [15–18]. Here we show that the hot-band absorption induced luminescence of such dyes can be enhanced by gold nanorods. We measured an enhancement factor of 350 for single Seta 670 molecules. Our findings open the potential of increasing the sensitivity of anti-Stokes luminescence-based imaging and extending single-molecule spectroscopy to a relatively unexplored type of luminescence.

4.2. Materials and methods

Materials. Spectroscopy grade methanol (99.9%) was purchased from Alfa Aesar. Seta 670 containing one reactive NHS-ester group (Seta-670-NHS) was purchased from SETA BioMedicals (Urbana, USA). Gold nanorods were from Nanopartz Inc. Their average dimensions were 38 nm $\times$ 118 nm as obtained from the transmission electron microscopy image provided by the manufacturer. Gold nanorods were immobilized onto a microscope coverslip with a spin-coating method described elsewhere [11, 19]. The coverslip was mounted in a home-made sample holder, where the dye solution can be added for further optical measurements. A second cover glass was placed immediately on top to prevent solvent evaporation.

Bulk absorption and fluorescence spectroscopy. UV-Vis absorbance measurements were performed using a Cary 50 spectrophotometer (Varian Analytical Instruments, USA). Bulk emission spectra in solution were recorded with a Cary Eclipse fluorescence spectrophotometer (Varian Analytical Instruments, USA). The temperature of the solutions in the cuvette was controlled by a single-cell Peltier accessory (Varian Analytical Instruments,

USA).

Single-particle spectroscopy was performed on a confocal microscopy setup described in detail in the Supporting Information. Briefly, we used a mode-locked titanium-sapphire laser (775 nm wavelength and 220 fs pulse width) with circular polarization to excite fluorescence from the molecules in a custom-built confocal microscope equipped with time-correlated single-photon counting (TCSPC) electronics (TimeHarp 200, PicoQuant GmbH, Berlin). For continuous-wave (CW) laser excitation, we switched the titanium-sapphire laser to the CW mode and kept the same wavelength. The laser wavelength is in resonance with the longitudinal plasmon of the nanorods (Fig. 4.4), generating a strongly enhanced local field for fluorescence enhancement. The plasmon resonance of each gold nanorod is determined by measuring the one-photon-excited photoluminescence spectrum excited by a 532-nm continuous-wave (CW) laser. Apart from more commonly used scattering spectra, photoluminescence spectra have been proven and used as an alternative method of measuring the plasmon resonances [20, 21].

Imaging and time trace recording. Immobilized nanorods were brought into the focus of the microscope and a typical area of 30 $\times$ 30 μm^2 was imaged with the Ti:Sapphire laser (see Fig. S4.6(c)). Gold nanorods were identified by their strong two-photon-excited photoluminescence. Figure S4.6 shows a typical spectrum of the two-photon-excited photoluminescence from a nanorod and the dependence of the luminescence intensity on the laser power. We selected only single gold nanorods which are evidenced by the Lorentzian one-photon photoluminescence spectral shape (measured with the 532-nm CW laser) for further measurements and analyses. Then a solution of 1 μM Seta 670 in methanol was applied to the sample. The titanium-sapphire laser was focused on the single nanorods and photons were recorded in time-ragged-time-resolved mode and further analyzed with SymPhoTime software. The autocorrelation analyses were performed with the raw single-photon data instead of the binned time traces.

4.3. Results and discussion

4.3.1. Optical characterization at room temperature

We first characterized the optical properties of Seta 670 by the bulk absorption and emission spectra measurements at room temperature. Figure 4.3(a) shows the UV-Vis absorption spectra of a diluted methanol solution (1 μM) of Seta 670. Seta 670 shows a narrow principal absorption band at 684 nm and a vibronic shoulder at around 630 nm. Strikingly, we observe that the emission spectrum of Seta 670 is dependent on the concentration of the solution. If the concentration is 1 μM or lower, the emission peak is at 704 nm, whereas the emission peak shifted to 720 nm when we increased the concentration to 100 μM (Fig. 4.2(a)). Figure S4.4 in the Supporting Information shows emission spectra measured with more concentrations, where the gradual red-shift is visualized when increasing the concentration. Such a concentration dependence is most probably a result of reabsorption due to the large overlap of the absorption and emission spectra [6].

We observed blue-shifted anti-Stokes emission from Seta 670 when exciting the long-energy tail of the absorption spectrum. Figure 4.2(b) shows the emission spectra of a 100 μM methanol solution of Seta 670 excited at 775 nm and 785 nm. The excitation was achieved

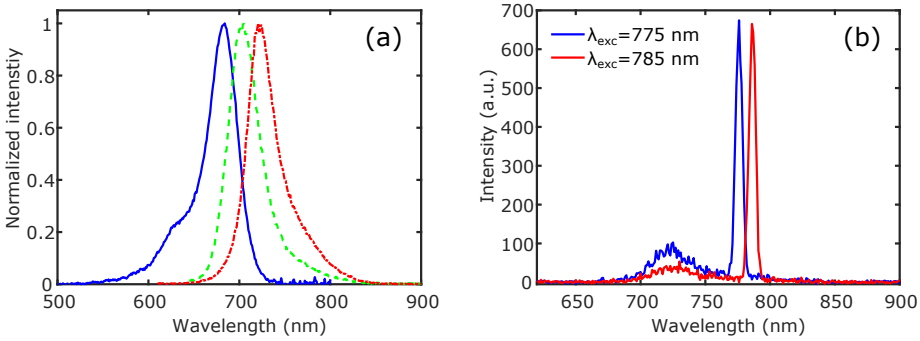

Figure 4.2: **Optical characterization of Seta 670 at room temperature**. (a) The blue solid line and dashed green line shows the absorption and Stokes fluorescence emission spectra of 1 μM Seta 670 in methanol, respectively. The red dot-dashed line shows the Stokes fluorescence emission spectrum of 100 μM Seta 670 in methanol. (b) Anti-Stokes luminescence spectra of Seta 670 (100 μM in methanol) excited at 775 nm and 785 nm. The high peaks at the excitation wavelengths were from the scattering of the solution.

by selecting the desired wavelength from the lamp of the spectrophotometer. An anti-Stokes emission peak at 720 nm was observed, irrespective of the excitation wavelength. The anti-Stokes emission wavelength is the same as the Stokes emission at the same concentration.

4.3.2. Temperature-dependent optical characterization

We then performed the temperature-dependent measurements to reveal the mechanism of anti-Stokes emission from Seta 670. Figure 4.3(a) shows the UV-Vis absorption spectra of 1 μM Seta 670 at different temperatures. The two absorption peaks do not shift upon temperature change. However, lower absorbance and broader spectra are seen as the temperature increases from 278.5 K to 333 K. There is a clear isosbestic point at $\sim$ 703 nm. Two other isosbestic points at $\sim$642 nm and $\sim$ 650 nm are less clear because they are too close to each other. See Fig. S4.3 for a zoom-in of the absorption spectra. The intensity decrease and spectral broadening were explained by Clark *et al.* with the Boltzmann distribution [6, 8]. Briefly, at low temperatures, most molecules tend to lie in the lowest possible state. As the temperature increases, the distribution over energy states becomes more uniform, so the absorption bands become broader in shape and lower in amplitude.

We then measured the fluorescence emission spectra of Seta 670 with an excitation wavelength of 650 nm. The dependence on temperature of the fluorescence spectra is shown on Fig. 4.3(a). This excitation wavelength was chosen because the absorbance at this wavelength does not dependent on the temperature. The princial emission band around 704 nm does not shift upon temperature change. The fluorescence intensity, however, decreases dramatically when the temperature was increased, which is attributed to the decrease of fluorescence quantum yield (QY) as the temperature was increased. We measured the quantum yield of the Stokes emission of Seta 670 at different temperatures (Fig. 4.3(b)). The quantum yield was determined using Seta 670 in pH 7.4 phosphate buffer as a reference sample with a known QY of 0.07 (at 298 K) provided by the manufacturer. The measured values

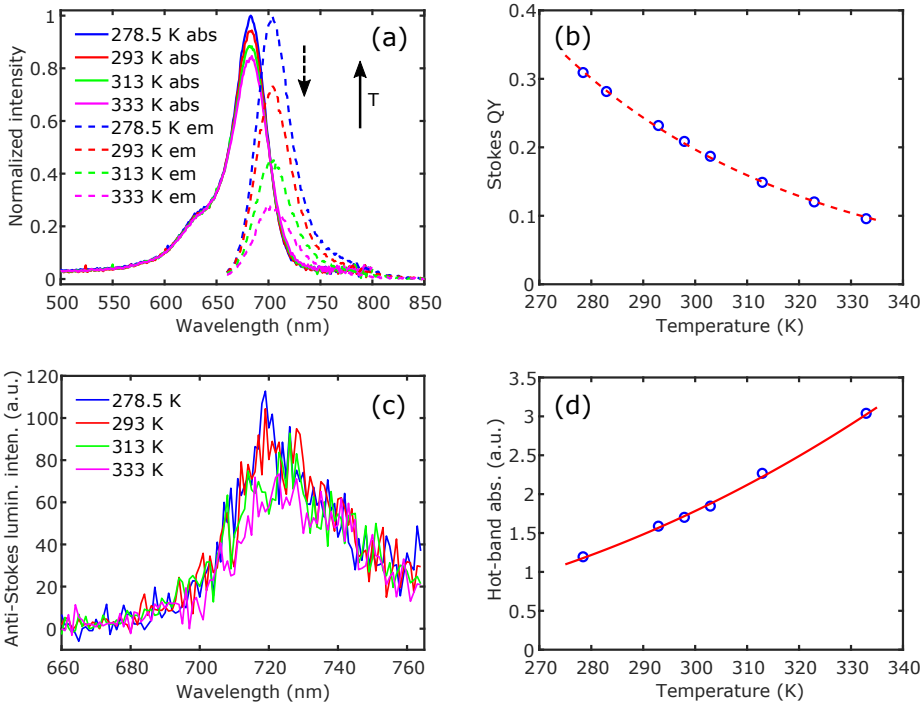

Figure 4.3: **Optical characterization of Seta 670**. (a) Absorption and Stokes fluorescence emission spectra of 1 μM Seta 670 in methanol at different temperatures. The absorption spectra have been normalized relative to the highest absorption spectrum and the emission spectra have been normalized relative to the highest emission spectrum. The excitation wavelength for the emission spectra was 650 nm. (b) Quantum yield of Stokes fluorescence of Seta 670 as a function of temperature. The dashed red line is an empirical exponential fit to the experimental data. (c) Anti-Stokes luminescence spectra of Seta 670 at different temperatures (λ_{exc} = 775 nm). (d) Hot-band absorption efficiency as a function of temperature (λ_{exc} = 775 nm). The red line shows an exponential fit to equation 4.1.

of quantum yield against temperature can be well fitted by an empirical single-exponential relation. The temperature dependent quantum yield is usually attributed to more efficient non-radiative processes related to thermal agitation at higher temperatures [22].

Figure 4.3(c) shows the emission spectra of a 100 μM methanol solution of Seta 670 at different temperatures (λ_{exc} = 775 nm). From Fig. 4.3(c) it is seen that the emission intensity of anti-Stokes increases slightly with decreasing temperature, which is not what we expect for hot-band absorption.This paradox can be solved by taking into account the temperature dependence of quantum yield shown in Fig.4.3(b). The lower anti-Stokes absorption at low temperatures is compensated by the higher quantum yield, resulting in a higher anti-Stokes emission. We divided the integrated anti-Stokes luminescence intensity by the quantum yield for the corresponding temperatures. The results are representative of the absorption efficiency at 775 nm (and the absolute values are not important). The absorption efficiency increases as the solution temperature increases (Fig. 4.3(d)). We fitted the results with an

exponential function:

$$I(T) = A\exp(-\Delta E/k_{\mathrm{B}}T), \tag{4.1}$$

where $I(T)$ is the relative hot-band absorption efficiency as a function of solution temperature T, k_{B} the Boltzmann constant, and A a proportionality coefficient. The thermal activation energy ΔE was determined from the fitting to be 138 meV, in good agreement with the difference between the excitation energy and the upconversion emission energy (134 meV). The anti-Stokes luminescence intensity excited with 785 nm was weaker than with 775 nm (Fig. 4.2(b)) due to the larger energy barrier. The results clearly confirms that the anti-Stokes emission from Seta 670 really originates from the optical excitation of a thermally populated vibration level (hot band).

4.3.3. Femtosecond laser excitation

Because of their donor-acceptor-donor structures, squaraine dyes have been found to have strong two-photon absorption and emission. The two-photon action cross-sections are comparable with those of semiconducotor quantum dots, whereas the size is much smaller than the latter [16, 23]. Therefore squaraine dyes have been proposed as promising fluorescent molecular probes in biological two-photon microscopy. Here we compared the blue-shifted emission excited with a CW laser (λ_{exc} = 775 nm) and that with a femtosecond pulsed laser (λ_{exc} = 775 nm) and found no evidence of two-photon-excited emission. As Fig. 4.4(a) illustrates, the intensity of emission under femtosecond excitation shows no difference from that under continuous-wave excitation at the same excitation power. Moreover, in both cases, the intensity of emission is a linear function of the excitation power. The blue spectrum shown in Fig. 4.4(b) shows the emission spectrum of Seta 670 excited with the femtosecond laser, which is identical with that excited with CW excitation. The results suggest that under our experimental conditions, the emission from Seta 670 with femtosecond pulsed excitation also stems from linear hot-band absorption. The contribution from two-photon absorption, if present at all, is negligible.

4.3.4. Enhancing hot-band absorption using gold nanorods

In the following, we used gold nanorods to enhance the upconversion luminescence of single Seta 670 molecules. We have proven that the anti-Stokes emission under CW and pulsed excitations stem from the same origin, so we used the pulsed laser to do the enhancement experiments with time-correlated single-photon counting electronics. The nanorods used in our study were the same as described in Chapter 2. The longitudinal surface plasmon resonance of the nanorods was 770 nm. For single-particle studies with the confocal microscope, the nanorods were well isolated and immobilized on a glass coverslip. The spectra of the nanorods exhibit good overlap with the excitation wavelength (775 nm) and some overlap with the emission of the dye, ensuring a high expected enhancement factor [11, 24].

Single isolated gold nanorods immobilized on a glass coverslip were immersed in a 1 μM methanol solution of Seta 670 and brought to the focus of the microscope. Figure 4.5(a) shows a typical time trace taken on a single nanorod, where signal bursts are identified. We attribute these bursts to enhanced anti-Stokes luminescence emission of single Seta 670 molecules when freely diffusing molecules approach the near field of the gold nanorod. The

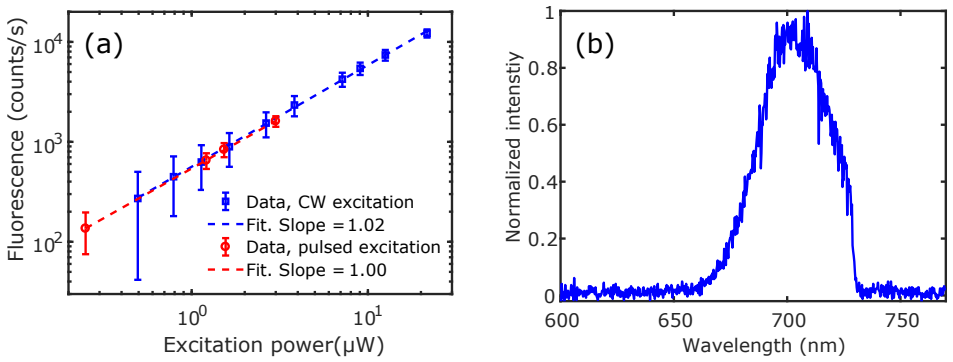

Figure 4.4: (a) Log-log plot showing the linear dependence of anti-Stokes emission of Seta 670 in methanol on the average excitation intensity under continuous-wave (blue) and pulsed (red) excitation. The wavelengths for continuous-wave and pulsed excitation were both 775 nm. The concentration of Seta 670 for the CW measurement was 1 μM. The concentration for the measurement with a pulsed laser was 5 μM and the fluorescence intensity has been scaled to 1 μM assuming a linear relation of fluorescence with concentration. (b) The emission spectrum of 5 μM Seta 670 in methanol excited by a 775-nm femtosecond laser. A 745-nm shortpass filter was used to cut the excitation wavelength.

corresponding autocorrelation is shown in Fig. 4.5(b). The autocorrelation is apparently non-exponential with no well-defined characteristic correlation time. Nevertheless, we fitted the autocorrelation to a single exponential and obtained a correlation time of 5.4 ms. As found out by previous works [10, 11, 24, 25], this correlation time is too long to be due to the free diffusion of molecules through the near field of a nanorod. It is most likely a result of the transient sticking (and subsequent photobleaching or desorption) of dye molecules to the glass substrate. The stretched decay behavior of the autocorrelation curve is attributable to the lack of a characteristic time scale for the non-specific sticking.

The background signal in the time trace, 3,800 counts/s, comes from all the unenhanced Seta 670 molecules in the focal volume and two-photon-excited luminescence of the nanorod. The contribution of dye molecules can be measured by recording a time trace on an area without a nanorod under the same experimental conditions. Such a time trace is also present in Fig. 4.5(a) with an average count rate of $\sim$ 1,000 counts/s. No significant fluorescence bursts higher than the photon noise can be seen. The corresponding autocorrelation curve shown in Fig. 4.5(b) does not show any correlation. This is expected because with a measured focal volume of 0.09 fL (Supporting Information) and a given dye concentration of 1 μM, we estimate on average 54 molecules in the focal volume. With such a high number of molecules, we do not expect any visible signal fluctuations above the experimental noise or any visible correlation contrast due to molecules diffusing in and out of the detection volume.

With the number molecules present in the detection volume, we can further estimate the average count rate of one molecule without enhancement to be 18.8 $\pm$ 0.2 counts/s. The count rate of the most intense signal burst (indicated by an arrow) shown in Fig. 4.5(a) is 10,400 counts/s against a background of 3,800 counts/s. This burst is due to the enhanced anti-Stokes luminescence emission, 6,600 counts/s, from a single Seta 670 molecule. Based on this, we can calculate an enhancement factor of 350.

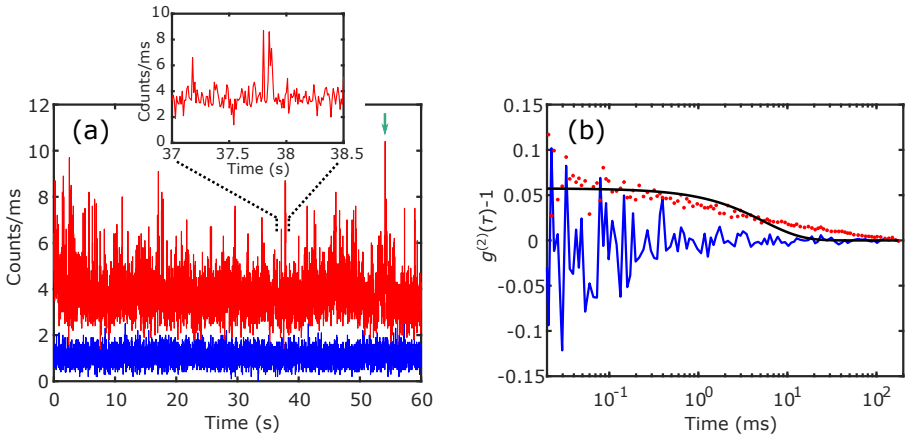

Figure 4.5: (a) Fluorescence time traces (10 ms per bin) taken on a nanorod (red dots) and on the background where no nanorod was present (blue line). The average excitation power of the pulsed laser was 1.5 μW at the sample. The inset figure is an expansion of part of the trace. (b) Autocorrelation curves of the measurements (colors correspond to (a)). The measurement on the background showed no correlation because of the high concentration of dye. An exponential fit (black solid line) to the red dots yields a correlation time of 5.4 ms, clearly longer than that takes for a molecule to diffuse through the near field of the nanorod.

4.4. Conclusion

In summary, we have characterized the hot-band absorption anti-Stokes luminescence of a squaraine dye. We have demonstrated the feasibility of enhancing anti-Stokes luminescence of single dye molecules using chemically synthesized gold nanorods. An enhancement factor of 350 was achieved by using nanorods with a plasmon resonance close to the excitation wavelength. Thanks to the sub-wavelength detection volume defined by the strong near field around the nanorods, fluorescence correlation spectroscopy could be performed even at a dye concentration of 1 μM, yielding a correlation time associated with the sticking or bleaching time of molecules on the glass substrate.

4.5. Supporting information

Schematic of the optical setup

Confocal microscopy measurements were performed on our home-built sample-scanning confocal fluorescence microscope (Fig. S4.1). A mode-locked titanium-sapphire laser (Coherent Mira 900) was made circularly polarized by a quarter-wave plate (not shown in the scheme) before entering the oil immersion objective (100×, NA = 1.4, Zeiss), and used for excitation. It was spatially filtered and expanded to overfill the aperture of the objective. The laser operated at 775 nm, 76 MHz repetition rate and 220 fs pulse width. The photoluminescence signal of Seta 670 molecules and/or gold nanorods collected by the same objective was filtered out from the back-scattered excitation light by a 745-nm short-pass filter (FF01-745/SP-25, Semrock) and a 785-nm notch filter (NF03-785E-25, Semrock). A multimode optical fiber with a core size of 62 μm was used as a confocal pinhole. A 532-

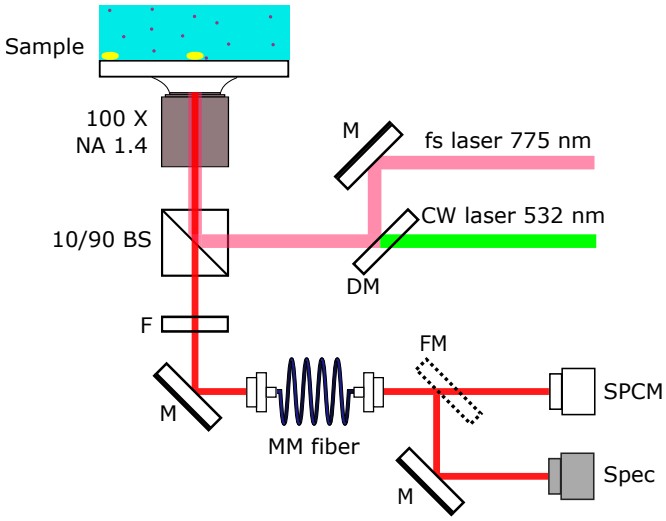

Figure S4.1: Schematic of the experimental setup for confocal microscopy and luminescence spectra measurements. BS - beam splitter, F - Set of filters: 745 nm short-pass filter + 785 notch filters for the titanium:sapphire laser or two 532 nm notch filters for the 532-nm laser, M - mirror, DM - dichroic mirror, FM - flip mirror, MM fiber - multimode fiber, SPCM - single-photon counting module, Spec - spectrometer. Waveplates and spatial filters are not shown in the scheme.

nm diode-laser-pumped solid-state continuous-wave laser (Shanghai Laser & Optics Century Co., Ltd), which matches the transverse plasmon resonance of nanorods, was used to measure the one-photon excited photoluminescence spectrum of each nanorod. For this, two 532-nm notch filters were used in place of the 745-nm shortpass and 785-nm notch filters. We used circular polarization to find nanorods regardless of their orientation. It was previously shown that nanorods' one-photon photoluminescence spectra closely resemble their scattering spectra [20], so photoluminescence is used to determine the resonance wavelengths. The near-infrared and green laser beams were overlapped with a shortpass dichroic mirror (FF720-SDi01-25×36, Semrock). Note that the two lasers were not used at the same time. We used a motorized flip mirror to direct luminescence either to a single-photon counting module (SPCM-AQR-16, PerkinElmer) or to a spectrometer equipped with a liquid-nitrogen-cooled CCD (Acton SP-500i, Princeton Instruments).

Size of the confocal volume

We measured the size of the confocal volume by measuring the point spread function (PSF) of the microscope [26]. We scanned sectional scattering images of an immobilized gold nanorod immersed in index-matching objective oil excited with the Ti:Sapphire laser. No detection filters were used. Figure S4.2 shows the *xz* section of the PSF (*z* is along the optical axis). All three sections (*xy*, *xz* and *yz*) of the PSF were fitted with two-dimensional Gaussian functions as described in Chapter 2. The size of the confocal volume is then calculated from the mean dimensions in each axis as

$$V_{\mathrm{conf}} = \left(\frac{\pi}{2}\right)^{3/2} w_x w_y w_z = 0.089 \pm 0.005 \text{ fL}, \tag{4.2}$$

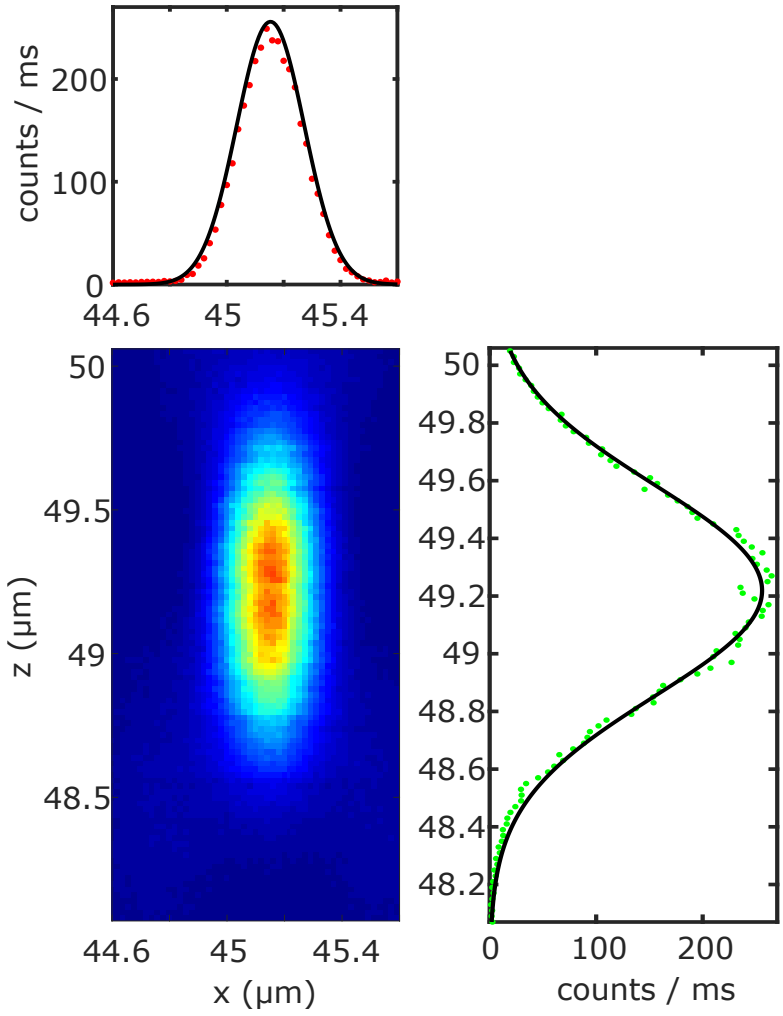

Figure S4.2: ***xz* section of the scattering PSF measured with a gold nanorod**. Line profiles through the center are shown. The red (along the x axis) and green (along the z axis) dots show the experimental data and the black lines represent two-dimensional Gaussian fits, which yield $w_x = 237.0 \pm 1.4$ nm and $w_z = 731.1 \pm 4.4$ nm.

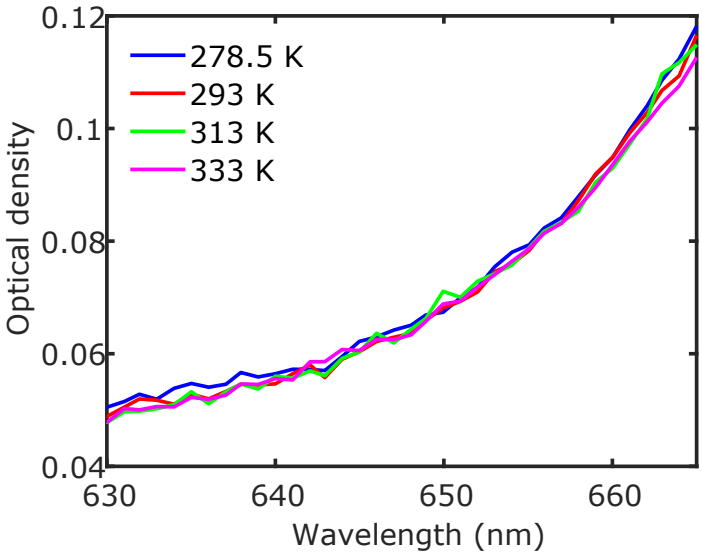

Figure S4.3: Detailed absorbance spectra of 1 μM Seta 670 as a function of temperature. It is a zoom-in plot of Fig. 4.3(a) in the main text. Two other isosbestic points at ∼642 nm and ∼ 650 nm are less clear because they are too close to each other.

where w_x, w_y and w_z are the $1/e^2$ radii along x, y and z axis, respectively.

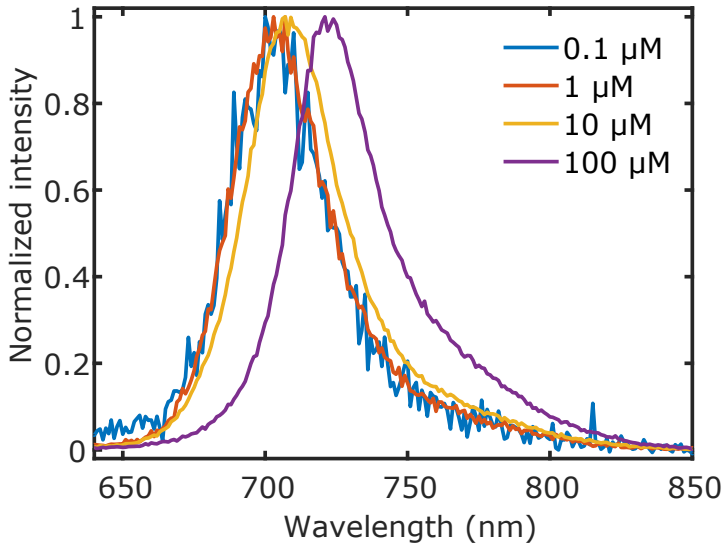

Figure S4.4: Concentration dependence of the Stokes fluorescence spectra of Seta 670. If the concentration is 1 μM or lower, the emission peak is at 704 nm. The emission peaks moves 710 nm if the concentration is increased to 10 muM. The 100 μM solution shows an emission peak at 720 nm. Such a concentration dependence is most probably a result of reabsorption due to the large overlap of the absorption and emission spectra [6].

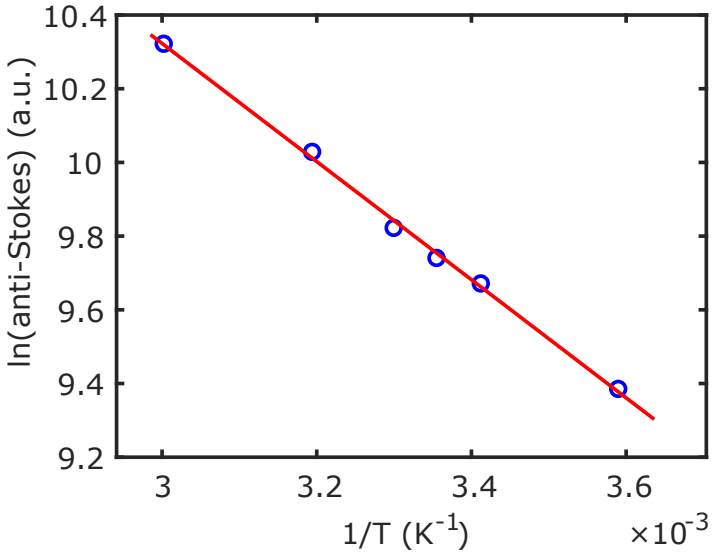

Figure S4.5: Linear plots of logarithm of integrated fluorescence intensity against inverse temperature of Seta 670 solution. The data are the same as shown in Fig. 4.3(d) in the main text but presented differently.

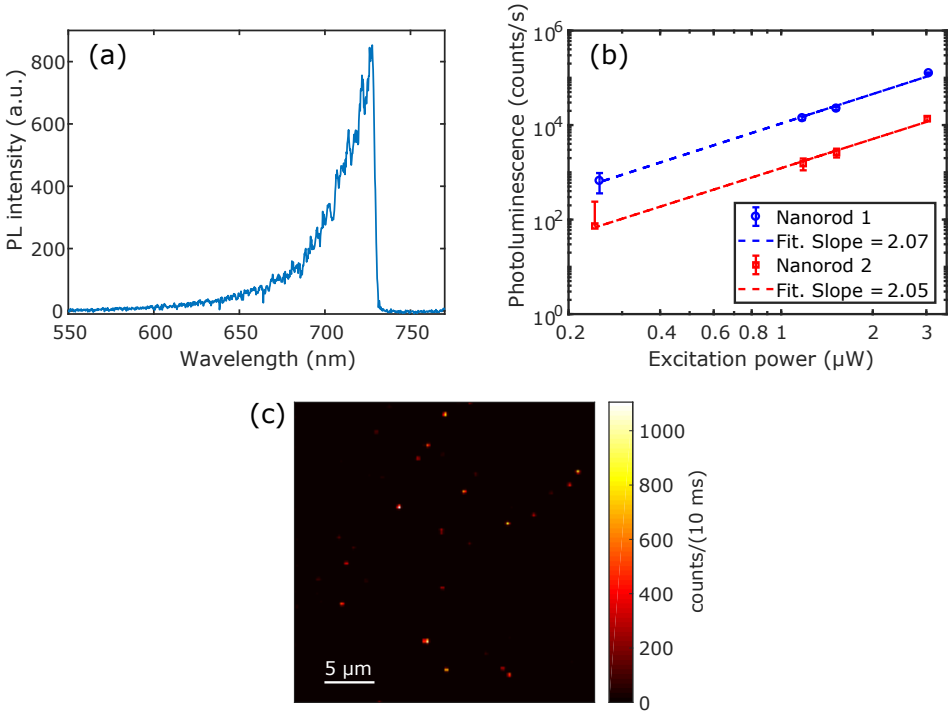

Figure S4.6: **Two-photon-excited luminescence of gold nanorods**. (a) Typical two-photon-excited luminescence spectrum of a gold nanorod immersed in water. The immobilized nanorod was excited with the femtosecond laser (circularly polarized) with an average power of 3 μW. (b) Log-log plot of the dependence of the photoluminescence intensity on the excitation power for two gold nanorods. The fitted slopes reveal a quadratic intensity-excitation relation, confirming the two-photon excitation origin of photoluminescence from the nanorods. The nanorods were immersed in methanol and excited with the femtosecond laser (circularly polarized). (c) An image of two-photon-excited luminescence of gold nanorods immobilized on a glass coverslip and immersed in methanol. The image size is 30 μm $\times$ 30 μm. Each pixel is 0.2 μm $\times$ 0.2 μm with an integration time of 10 ms/pixel. The excitation source was the femtosecond laser (circularly polarized) with an average power of 3 μW. For (a-c), a 745-nm shortpass filter and a 785-nm notch filter were used to block the excitation wavelength.

References

[1] M. Orrit and J. Bernard, *Single pentacene molecules detected by fluorescence excitation in a p-terphenyl crystal,* Physical Review Letters **65**, 2716 (1990).

[2] B. Schuler and W. A. Eaton, *Protein folding studied by single-molecule FRET,* Current Opinion in Structural Biology **18**, 16 (2008).

[3] S. Weiss, *Fluorescence spectroscopy of single biomolecules,* Science **283**, 1676 (1999).

[4] X. S. Xie and H. P. Lu, *Single-molecule enzymology,* Journal of Biological Chemistry **274**, 15967 (1999).

[5] X. Zhu, Q. Su, W. Feng, and F. Li, *Anti-Stokes shift luminescent materials for bioapplications,* Chemical Society Reviews **46**, 1025 (2017).

[6] J. L. Clark, P. F. Miller, and G. Rumbles, *Red edge photophysics of ethanolic rhodamine 101 and the observation of laser cooling in the condensed phase,* The Journal of Physical Chemistry A **102**, 4428 (1998).

[7] W. Qin, S. Huang, G. Du, J. Zhang, G. De, J. Zhang, Y. Wang, C. Cao, and S. Lu, *Anti-Stokes fluorescent cooling by energy transfer,* Journal of Luminescence **119**, 356 (2006).

[8] Y. Liu, Q. Su, X. Zou, M. Chen, W. Feng, Y. Shi, and F. Li, *Near-infrared in vivo bioimaging using a molecular upconversion probe,* Chemical Communications **52**, 7466 (2016).

[9] P. Anger, P. Bharadwaj, and L. Novotny, *Enhancement and quenching of single-molecule fluorescence,* Physical Review Letters **96**, 113002 (2006).

[10] A. Kinkhabwala, Z. Yu, S. Fan, Y. Avlasevich, K. Müllen, and W. Moerner, *Large single-molecule fluorescence enhancements produced by a bowtie nanoantenna,* Nature Photonics **3**, 654 (2009).

[11] H. Yuan, S. Khatua, P. Zijlstra, M. Yorulmaz, and M. Orrit, *Thousand-fold enhancement of single-molecule fluorescence near a single gold nanorod,* Angewandte Chemie International Edition **52**, 1217 (2013).

[12] Y. Fu, J. Zhang, and J. R. Lakowicz, *Plasmon-enhanced fluorescence from single fluorophores end-linked to gold nanorods,* Journal of the American Chemical Society **132**, 5540 (2010).

[13] S. A. Maier, *Plasmonics: fundamentals and applications* (Springer Science & Business Media, 2007).

[14] F. Tam, G. P. Goodrich, B. R. Johnson, and N. J. Halas, *Plasmonic enhancement of molecular fluorescence,* Nano Letters **7**, 496 (2007).

[15] S. Sreejith, P. Carol, P. Chithra, and A. Ajayaghosh, *Squaraine dyes: a mine of molecular materials,* Journal of Materials Chemistry **18**, 264 (2008).

[16] K. Podgorski, E. Terpetschnig, O. P. Klochko, O. M. Obukhova, and K. Haas, *Ultra-bright and stable red and near-infrared squaraine fluorophores for in vivo two-photon imaging,* PloS one **7**, e51980 (2012).

[17] E. G. Matveeva, E. A. Terpetschnig, M. Stevens, L. Patsenker, O. S. Kolosova, Z. Gryczynski, and I. Gryczynski, *Near-infrared squaraine dyes for fluorescence enhanced surface assay,* Dyes and Pigments **80**, 41 (2009).

[18] E. Arunkumar, N. Fu, and B. D. Smith, *Squaraine-derived rotaxanes: Highly stable, fluorescent near-IR dyes,* Chemistry-A European Journal **12**, 4684 (2006).

[19] W. Zhang, M. Caldarola, B. Pradhan, and M. Orrit, *Gold nanorod enhanced fluorescence enables single-molecule electrochemistry of methylene blue,* Angewandte Chemie International Edition **56**, 3566 (2017).

[20] M. Yorulmaz, S. Khatua, P. Zijlstra, A. Gaiduk, and M. Orrit, *Luminescence quantum yield of single gold nanorods,* Nano Letters **12**, 4385 (2012).

[21] A. Carattino, S. Khatua, and M. Orrit, *In situ tuning of gold nanorod plasmon through oxidative cyanide etching,* Physical Chemistry Chemical Physics **18**, 15619 (2016).

[22] B. Valeur and M. N. Berberan-Santos, *Molecular fluorescence: principles and applications* (John Wiley & Sons, 2012).

[23] S.-J. Chung, S. Zheng, T. Odani, L. Beverina, J. Fu, L. A. Padilha, A. Biesso, J. M. Hales, X. Zhan, K. Schmidt, A. Ye, E. Zojer, S. Barlow, D. J. Hagan, E. W. Van Stryland, Y. Yi, Z. Shuai, G. A. Pagani, J.-L. Brédas, J. W. Perry, and S. R. Marder, *Extended squaraine dyes with large two-photon absorption cross-sections,* Journal of the American Chemical Society **128**, 14444 (2006).

[24] S. Khatua, P. M. Paulo, H. Yuan, A. Gupta, P. Zijlstra, and M. Orrit, *Resonant plasmonic enhancement of single-molecule fluorescence by individual gold nanorods,* ACS Nano **8**, 4440 (2014).

[25] S. Khatua, H. Yuan, and M. Orrit, *Enhanced-fluorescence correlation spectroscopy at micro-molar dye concentration around a single gold nanorod,* Physical Chemistry Chemical Physics **17**, 21127 (2015).

[26] S. Rüttinger, V. Buschmann, B. Krämer, R. Erdmann, R. Macdonald, and F. Koberling, *Comparison and accuracy of methods to determine the confocal volume for quantitative fluorescence correlation spectroscopy,* Journal of Microscopy **232**, 343 (2008).